# Interface Elements in Global/Local Analysis – Part 3: Shell-to-Solid Transition

John E. Schiermeier
Senior Development Engineer
The MacNeal-Schwendler Corporation
Los Angeles, California

Rajendra K. Kansakar
Senior Software Engineer
The MacNeal-Schwendler Corporation
Los Angeles, California

Jonathan B. Ransom
NASA Langley Research Center
Hampton, Virginia

Mohammad A. Aminpour
Applied Research Associates, Inc.
Hampton, Virginia

W. Jefferson Stroud
NASA Langley Research Center
Hampton, Virginia

The 1999 MSC Worldwide Aerospace Conference
Long Beach, California
June 7-10, 1999

## Abstract

When performing global/local analysis, the issue of connecting dissimilar meshes often arises, especially when refinement is performed. One method of connecting these dissimilar meshes is to use interface elements. In the previous Parts 1 and 2, curve and surface interface elements, implemented for p-element edges and faces in MSC/NASTRAN Versions 69 and 70.5, respectively, were presented. In the current Part 3, the shell-to-solid transition interface element, being implemented to connect dissimilar p-element edges with p-element faces, is presented with examples. This transition interface element completes the set of interface tools for global/local analysis.

# 1 Introduction

The problem of connecting dissimilar meshes at a common interface is a major one in finite element analysis. One method of connecting these dissimilar meshes is to use interface elements.

The first paper, Part 1 [1], described the curve interface elements implemented in Version 69 of MSC/NASTRAN for shell and beam p-element edges. The background, theory, implementation, and examples were also presented. The second paper, Part 2 [2], described the surface interface elements implemented in Version 70.5 of MSC/NASTRAN for solid and shell p-element faces. The background, theory, implementation, and examples were also presented. The current paper, Part 3, describes the shell-to-solid transition interface elements being implemented in MSC/NASTRAN for solid p-element faces and shell p-element edges. The background, theory, and implementation are very similar to the previous parts and will be repeated and extended here. Examples will also be presented.

## *1.1 Applications*

Dissimilar meshes can arise with global/local analysis, where part of the structure is modeled as the area of primary interest, in which detailed stress distributions are required, and part of the structure is modeled as the area of secondary interest, through which load paths are passed into the area of primary interest. Generally the area of primary interest has a finer mesh than the area of secondary interest, and therefore a transition area is required. Severe transitions generally produce elements that are heavily distorted, which can result in poor stresses and poor load transfer into the area of primary interest. Patches of elements may be removed from the global model and replaced by denser patches for local detail. An example is shown in Figure 1, where the boundaries of the patches are bold. In addition, the local elements may have a more complicated topology than the global elements.

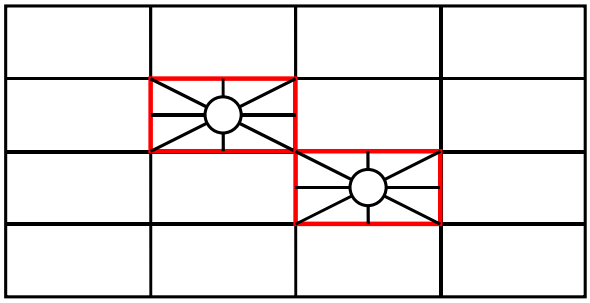

**Figure 1: Example of Dissimilar Mesh from Global/Local Analysis.**

In large system problems, different analysts or even different organizations may have created different components of the model, such as the wing and the fuselage of an airplane. Unless they have carefully coordinated their efforts, the finite element meshes of the different components may not match at the interfaces, as normally required, when they are assembled.

Dissimilar meshes can be created by automeshers, which may be required to transition between large elements and small elements in a limited area. An example is shown in Figure 2, where the boundary is bold and the required transition is dashed. Many automeshers generate tetrahedral meshes for solids, and distorted tetrahedra may be more susceptible to poor results. Automeshers are often used in conjunction with shape optimization procedures, where the shape changes are large enough to warrant remeshing. In these cases, it would be more efficient to remesh only the local part of the model and interface it with the rest, rather than remeshing the entire model. If the rest of the model has not been remeshed, then the associated parts of the stiffness matrix need not be recalculated, provided that the previous data has been saved.

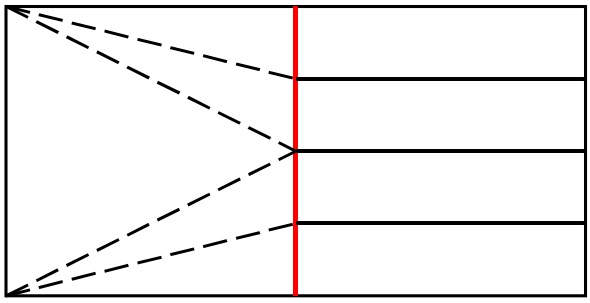

**Figure 2: Example of Dissimilar Mesh from Automesher.**

In h-refinement, subdivided elements may be adjacent to undivided elements. Without some kind of interface element, the subdivision would have to be extended to the model boundary or otherwise transitioned. An example is shown in Figure 3, where the boundary is bold and the required transitions are dashed.

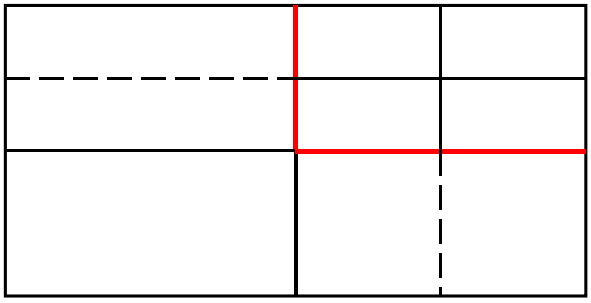

**Figure 3: Example of Dissimilar Mesh from h-Refinement.**

### *1.2 Previous Methods*

Much work has been done to resolve the element interface problem, with most of the efforts concentrating on moving the nodes or writing multi-point constraint (MPC) equations on the interfaces. The first approach, moving the nodes, must take into account the element distortions on both sides of the interface and provide the best redistribution according to some criteria. However, it is possible that one or both sides of the interface may be represented only by previously generated stiffness matrices, in which case the

nodes cannot be moved. The biggest restriction of moving nodes is that both sides of the interface must have the same number and type of elements. Therefore, this method is not practical for the general problem.

The second approach, using MPC equations, often is used for connecting elements of different types. For example, the midside node of a quadratic element may be constrained to move linearly with the vertex nodes in order to match an adjacent linear element, assuming that the vertex nodes for the two elements are coincident. Other MPC equations, such as splines, can handle more general cases. However, MPC equations by definition provide additional relationships for the existing degrees of freedom on the interface, and in the process reduce the number of independent degrees of freedom. If there are no degrees of freedom created, this could result in additional local stiffness or other non-physical effects in the model.

### *1.3 Current Method*

The need and applications for reliable interface technology are great. NASA Langley Research Center has developed a method for analyzing structures composed of two or more independently modeled substructures, based on a hybrid variational formulation with Lagrange multipliers, and applied it to global/local demonstration problems for one-dimensional [3-6] and two-dimensional [7] interfaces. NASA has also developed the technology for a solid-to-shell transition element for use with composites [8], and has combined it with the one-dimensional interface element [8].

Under terms of a cooperative agreement between MSC and NASA [9], MSC has extended and implemented this interface technology into MSC/NASTRAN for p-element edges along a geometric curve, and for p-element faces over a geometric surface. Currently MSC is implementing the transition interface technology for solid p-element faces and shell p-element edges. This agreement is part of NASA's continuing effort to transfer technology into the mainstream of industry as an aid in developing competitiveness in the worldwide market.

## 2 Implementation

The purpose of the shell-to-solid transition interface element is to connect a set of solid p-element faces with a set of shell p-element edges, as shown in Figure 4, where the boundary is bold:

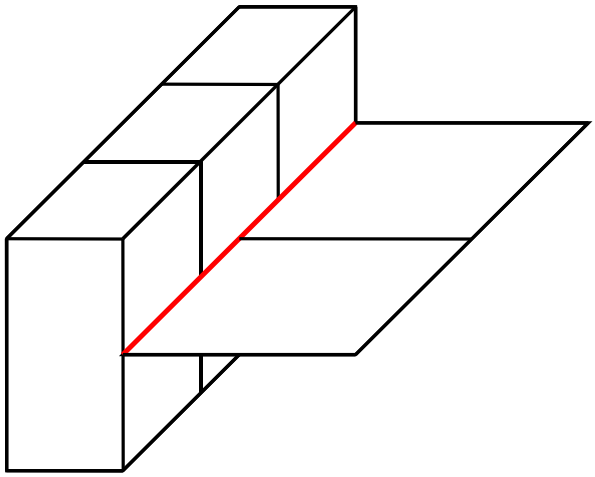

**Figure 4: Shell-to-Solid Transition Interface Element.**

Neither the curve interface element (GMINTC), which interfaces p-element edges along a common curve, nor the surface interface element (GMINTS), which interfaces p-element faces over a common surface, has kinematic constraints to connect the shell degrees of freedom to the solid. Both also connect only entities of the same topological type. The shell-to-solid element connector (RSSCON) models clamped connection of shells to solids by generating multi-point constraints with the shell degrees of freedom in the dependent set [10]. However, it requires that the shell p-element mesh must align with the solid p-element mesh with exact element-to-element correspondence.

Given these restrictions, it is possible to combine the GMINTC with the RSSCON to create a shell-to-solid transition interface element. In order to accomplish this, a transition boundary, with both translations and rotations, is created, as shown in Figure 5. This transition boundary maintains the element-to-element correspondence with the solid p-element faces, so that the RSSCON can connect it with the solid p-elements, and consists of p-element edges, so that the GMINTC can connect it with the shell p-elements.

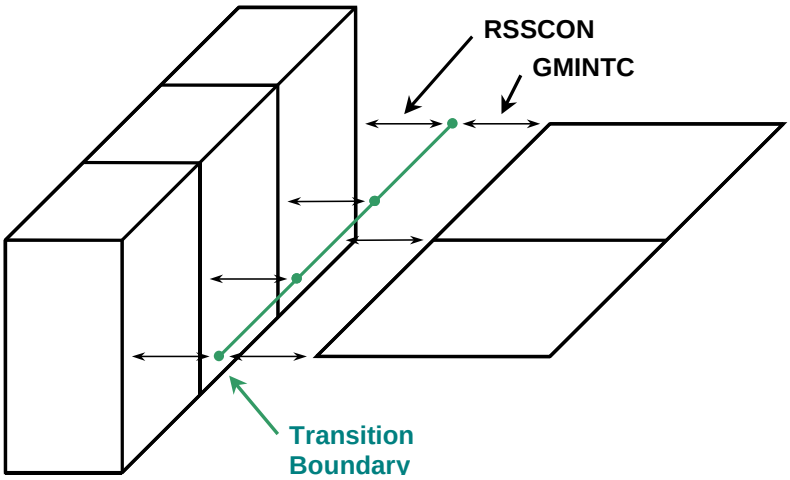


**Figure 5: Transition Boundary (exploded view).**

Since this is a more general form of the RSSCON, the RSSCON bulk data entry is being enhanced [10]. There is another option, INTC, being added to the RSSCON, and for this option, the required input is the boundary of shell p-element edges (GMBNDC) [1], the boundary of solid p-element faces (GMBNDS) [2], and the curve interface properties (PINTC) [1].

# 3 Formulation

Given the implementation of the shell-to-solid transition interface element, the formulation consists of two parts. First is the formulation of the interface element, and second is the formulation of the transition element.

## *3.1 Interface Element*

The formulation of the interface element, which is a hybrid variational formulation using Lagrange multipliers, is defined in summary as follows, using primarily the notation in [3]. It is repeated in more general form here to include the dynamic case. The complete details for the static case may be found in [3-5,7].

The displacement vector $\{v\}$ on the interface is defined in terms of the node and edge coefficients $\{q_s\}$, which are defined on the interface elements, and interpolation functions $[T]$, which is a matrix containing the functions for each field of the interface displacement vector:

$$\{v\} = [T]\{q_s\}$$

The displacement vector $\{u_j\}$ on each subdomain $j$ is defined in terms of the node and edge coefficients $\{q_j\}$ and interpolation functions $[N_j]$, which is a matrix containing the functions for each field of the subdomain displacement vector:

$$\{u_j\} = [N_j]\{q_j\}$$

The Lagrange multiplier vector $\{\lambda_j\}$ on each subdomain $j$ is defined in terms of the node and edge coefficients $\{\alpha_j\}$ and interpolation functions $[R_j]$, which is a matrix containing the functions for each field of the Lagrange multiplier vector:

$$\{\lambda_j\} = [R_j]\{\alpha_j\}$$

Defining the combined operator and material matrix $[B_j]$, the density $\rho$, and the surface tractions $\{t_j\}$; and considering the potential energy for all the subdomains $j$ with the internal energy, inertial forces, and applied forces, and for the interface $I$ with the Lagrange multipliers; gives:

$$\Pi = \sum_j \left[ \tfrac{1}{2} \int_\Omega u_j^T \, B_j \, u_j \, dA + \tfrac{1}{2} \int_\Omega u_j^T \, \rho_j \, \ddot{u}_j \, dA - \int_\Gamma u_j^T \, t \, ds + \int_I \lambda_j^T \left( v - u_j \right) ds \right]$$

where the inertial body forces:

$$F_j = -\rho_j \, \ddot{u}_j$$

have been multiplied by a factor of one half since they are proportional loads. Using the standard assumption of simple harmonic motion for the frequency $\omega$:

$$\ddot{u}_j = -\omega^2 \, u_j$$

and expanding the vectors into their coefficients and interpolation functions gives:

$$\Pi = \sum_j \left[ \tfrac{1}{2} \int_\Omega q_j^T \, N_j^T \, B_j \, N_j \, q_j \, dA - \tfrac{1}{2} \int_\Omega q_j^T \, N_j^T \, \rho_j \, \omega^2 \, N_j \, q_j \, dA - \int_\Gamma q_j^T \, N_j^T \, t_j \, ds \right.$$
$$\left. + \int_I \left( q_s^T \, T^T - q_j^T \, N_j^T \right) R_j \, \alpha_j \, ds \right]$$

Defining the matrices of interpolation functions:

$$M_j = -\int_I N_j^T \, R_j \, ds$$

$$G_j = \int_I T^T \, R_j \, ds$$

and substituting these, together with the standard definition of stiffness matrices $\lfloor k_j \rfloor$, mass matrices $\lfloor m_j \rfloor$, and load vectors $\{ f_j \}$, into the potential energy gives:

$$\Pi = \sum_j \left[ \tfrac{1}{2} \, q_j^T \, k_j \, q_j - \tfrac{1}{2} \, \omega^2 \, q_j^T \, m_j \, q_j - q_j^T \, f_j + \left( q_s^T G_j - q_j^T \, M_j \right) \alpha_j \right]$$

Partitioning the $q$ into $q^i$, those node and edge coefficients on the interface, and $q^o$, those coefficients other than on the interface, gives:

$$\Pi = \sum_j \left\{ \tfrac{1}{2} \begin{bmatrix} q_j^{oT} & q_j^{iT} \end{bmatrix} \begin{bmatrix} k_j^{oo} & k_j^{oi} \\ k_j^{io} & k_j^{ii} \end{bmatrix} \begin{Bmatrix} q_j^o \\ q_j^i \end{Bmatrix} - \tfrac{1}{2} \, \omega^2 \begin{bmatrix} q_j^{oT} & q_j^{iT} \end{bmatrix} \begin{bmatrix} m_j^{oo} & m_j^{oi} \\ m_j^{io} & m_j^{ii} \end{bmatrix} \begin{Bmatrix} q_j^o \\ q_j^i \end{Bmatrix} \right.$$
$$\left. - \begin{bmatrix} q_j^{oT} & q_j^{iT} \end{bmatrix} \begin{Bmatrix} f_j^o \\ f_j^i \end{Bmatrix} + \left( \lfloor q_s^T \rfloor [G_j] - \lfloor q_j^{iT} \rfloor [M_j] \right) \{ \alpha_j \} \right\}$$

Deriving the Euler equations by taking the variations of the potential energy with respect to the four groups of variables $q_j^o$, $q_j^i$, $q_s$, and $\alpha_j$ gives:

$$\frac{\partial \Pi}{\partial q_j^o} = \left( k_j^{oo} - \omega^2 \, m_j^{oo} \right) q_j^o + \left( k_j^{oi} - \omega^2 \, m_j^{oi} \right) q_j^i - f_j^o = 0$$

$$\frac{\partial \Pi}{\partial q_j^i} = \left( k_j^{io} - \omega^2 \, m_j^{io} \right) q_j^o + \left( k_j^{ii} - \omega^2 \, m_j^{ii} \right) q_j^i - f_j^i + M_j \, \alpha_j = 0$$

$$\frac{\partial \Pi}{\partial q_s} = \sum_j G_j \, \alpha_j = 0$$

$$\frac{\partial \Pi}{\partial \alpha_j} = G_j^T \, q_s + M_j^T \, q_j^i = 0$$

Each of the Euler equations has a physical interpretation. Writing the Euler equations in matrix form:

$$\left( \begin{bmatrix} k_j^{oo} & k_j^{oi} & \cdots & 0 & 0 & \cdots \\ k_j^{io} & k_j^{ii} & \cdots & 0 & M_j & \cdots \\ \vdots & \vdots & & \vdots & \vdots & \\ 0 & 0 & \cdots & 0 & G_j & \cdots \\ 0 & M_j^T & \cdots & G_j^T & 0 & \cdots \\ \vdots & \vdots & & \vdots & \vdots & \end{bmatrix} - \omega^2 \begin{bmatrix} m_j^{oo} & m_j^{oi} & \cdots & 0 & 0 & \cdots \\ m_j^{io} & m_j^{ii} & \cdots & 0 & 0 & \cdots \\ \vdots & \vdots & & \vdots & \vdots & \\ 0 & 0 & \cdots & 0 & 0 & \cdots \\ 0 & 0 & \cdots & 0 & 0 & \cdots \\ \vdots & \vdots & & \vdots & \vdots & \end{bmatrix} \right) \begin{Bmatrix} q_j^o \\ q_j^i \\ \vdots \\ q_s \\ \alpha_j \\ \vdots \end{Bmatrix} = \begin{Bmatrix} f_j^o \\ f_j^i \\ \vdots \\ 0 \\ 0 \\ \vdots \end{Bmatrix}$$

This system of equations is symmetric, but not positive definite. All of the interface terms $\lfloor M_j \rfloor$ and $\lfloor G_j \rfloor$ appear in the stiffness matrix, with none in the mass matrix. Had damping been included, which generally takes the form of a load proportional to the velocity, the result would have been similar.

### *3.2 Transition Element*

The formulation of the transition element, which is based on the Reissner-Mindlin assumptions, is defined in summary as follows, using primarily the notation in [8]. The formulation for p-elements is an extension of that developed in [8].

The standard Reissner-Mindlin kinematic assumptions, where *x* and *y* are the membrane directions and *z* is the normal direction of the shell, are given by [8]:

$$u_x(x,y,z) = u(x,y) + z\,\theta_y(x,y)$$
$$u_y(x,y,z) = v(x,y) - z\,\theta_x(x,y)$$
$$u_z(x,y,z) = w(x,y)$$

Rearranging and linear interpolating these terms, where *a* and *b* refer to the lower and upper solid surfaces, respectively, and *c* to the shell surface, and where $\lambda$ is the fractional distance of the shell surface from the lower to the upper solid surface:

$$\lambda = \frac{(z^c - z^a)}{(z^b - z^a)}$$

yields:

$$u^c = (1-\lambda)\,u_x^a + \lambda\,u_x^b \qquad \theta_x^c = -\frac{(u_y^b - u_y^a)}{(z^b - z^a)}$$
$$v^c = (1-\lambda)\,u_y^a + \lambda\,u_y^b$$
$$w^c = (1-\lambda)\,u_z^a + \lambda\,u_z^b \qquad \theta_y^c = \frac{(u_x^b - u_x^a)}{(z^b - z^a)}$$

These equations are applied as multi-point constraints on the node coefficients for the transition element, where the $u^c$, $v^c$, $w^c$, $\theta_x^c$, and $\theta_y^c$ displacements correspond to the displacement vector $\{v\}$ in the previous section. For the p-element transition, they must also be applied to the hierarchic edge coefficients in a distributed manner.

# 4 Example Problems

Several sets of example problems were analyzed, in order to test the capabilities of the shell-to-solid transition interface element with various boundary meshes. The transition interface element uses two levels of approximation. The goal of the interface is that it should not decrease the accuracy below that obtained using the less refined boundary with a conforming mesh. However, it will not increase the accuracy above that obtained using the more refined boundary with a conforming mesh. The goal of the transition is that it should not decrease the accuracy below the Reissner-Mindlin assumptions. However, it will not increase the accuracy above that using a solid mesh. Therefore these restrictions must be considered when looking at results.

## *4.1 Patch Test*

The first example problem is a patch test, originally proposed in [11] and modified in [8] for the transition interface. The problem was further modified here, subdividing the center solid element into four elements, to make the interface non-conforming, as shown in Figure 6.

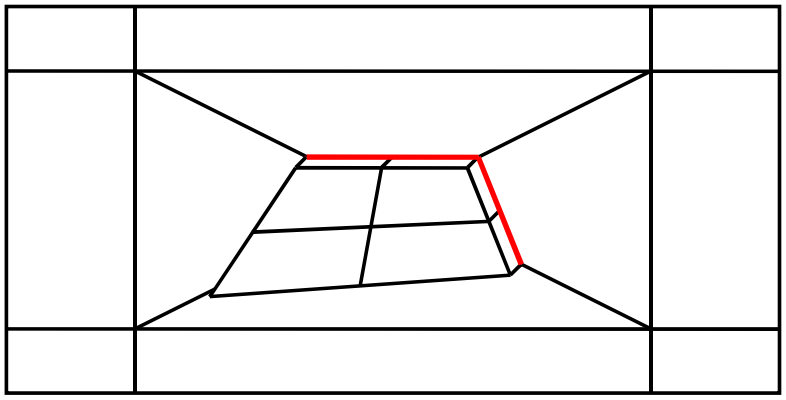

**Figure 6: Patch Test.**

The goal of the patch test is to show that the elements, in this case particularly the transition interface, can reproduce various stress states exactly with distorted elements. For this problem, a linearly varying displacement is prescribed around the entire boundary:

$$u(x,y) = 10^{-3} \cdot (x + y/2)$$
$$v(x,y) = 10^{-3} \cdot (y + x/2)$$

which leads to the uniform state of stress:

$$\varepsilon_x = \varepsilon_y = \gamma_{xy} = 10^{-3}$$
$$\sigma_x = \sigma_y = 1333.$$
$$\tau_{xy} = 400.0$$

The displacement contours and the von Mises stress contours are shown in Figure 7.

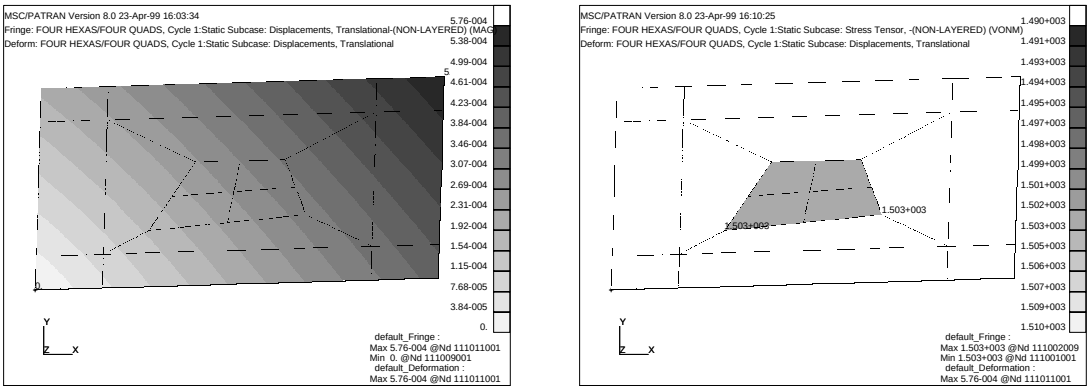


**Figure 7: Displacement and Stress Contours for Patch Test (p=3).**

The displacement contours show exactly the applied displacement field, with no breaks for the interface elements. The von Mises stress contours are constant with a value of 1503, which is also the exact value. Each of the individual stress components is exact as well, as shown in Table 1. While this is not a sufficient test, it is a necessary one.

**Table 1: Stress Components for Patch Test (p=3).**

| Stress component | Minimum | Maximum |
|---|---|---|
| $\sigma_x$ | 1333. | 1333. |
| $\sigma_y$ | 1333. | 1333. |
| $\tau_{xy}$ | 400.0 | 400.0 |

### *4.2 Cantilever Plate*

The second example problem is a cantilever plate that has exact solutions at low p-levels. The boundaries for each of the meshes are shown in Figure 8, with the solid p-element faces on the left and the shell p-elements on the right of each diagram. Some of the meshes serve as baselines for the transition interface and use an interface element, even though they are conforming.

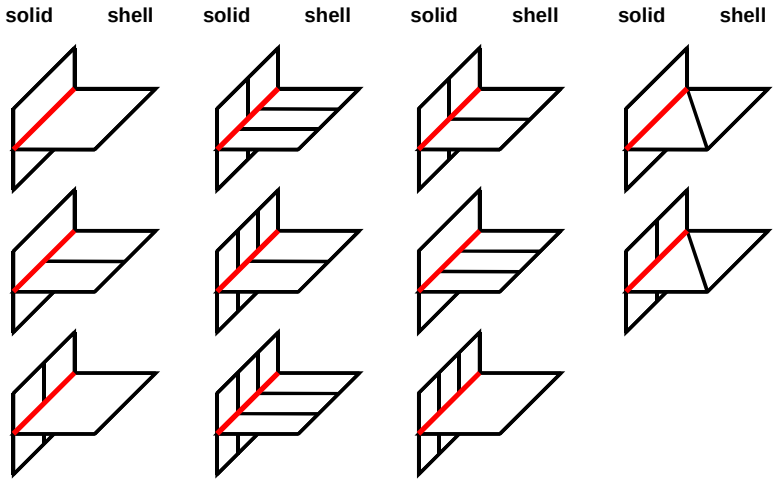


**Figure 8: Boundaries on Cantilever Plates.**

Tension (exact at p=1), moment (exact at p=2), in-plane shear (exact at p=3), out-of-plane shear (exact at p=3), and torsion (no exact answer) load cases were analyzed. The displacement contours at p=3 for the in-plane shear and torsion load cases with the one hexa/one quad mesh are shown on the deformed shape in Figure 9. The maximum displacement values are also printed at the appropriate locations. Since this mesh is conforming, it serves as a benchmark and provides a verification of the transition interface.

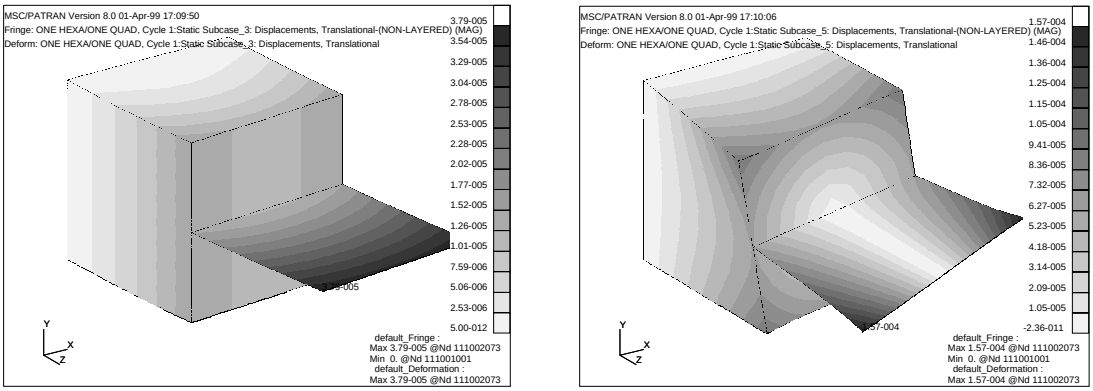


**Figure 9: Displacement Contours on Cantilever Plate (p=3).**

The displacement contours at p=3 for the in-plane shear and torsion load cases with the three hexa/two quad mesh are shown on the deformed shape in Figure 10. This mesh is not conforming, and may be compared with the benchmark solution for accuracy.

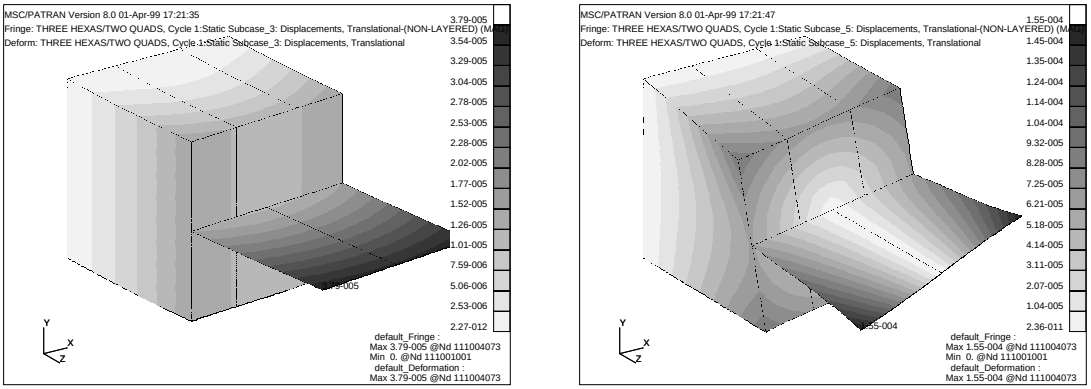


**Figure 10: Displacement Contours on Cantilever Plate (p=3).**

The maximum values of the displacement at p=3 for each of the five load cases are listed in Table 2 for all meshes. All of the meshes are exact for the theoretical load cases and differ for the torsion load case. The answers for the torsion load case differ because of the relatively low p=3; at higher p-levels the answers should converge. Note that they may converge to a solution limited by the Reissner-Mindlin assumptions, not the exact solution, because of the errors of idealization.

**Table 2: Maximum Displacement for Cantilever Plate (p=3).**

| Mesh | Tension $\times 10^{-5}$ | Moment $\times 10^{-4}$ | In-shear $\times 10^{-5}$ | Out-shear $\times 10^{-4}$ | Torsion $\times 10^{-4}$ |
|---|---|---|---|---|---|
| one hexa/one quad | 2.000 | 2.400 | 3.600 | 3.640 | 1.568 |
| one hexa/two quads | 2.000 | 2.400 | 3.600 | 3.640 | 1.550 |
| two hexas/one quad | 2.000 | 2.400 | 3.600 | 3.640 | 1.567 |
| two hexas/two quads | 2.000 | 2.400 | 3.600 | 3.640 | 1.552 |
| one hexa/three quads | 2.000 | 2.400 | 3.600 | 3.640 | 1.547 |
| three hexas/one quad | 2.000 | 2.400 | 3.600 | 3.640 | 1.569 |
| two hexas/three quads | 2.000 | 2.400 | 3.600 | 3.640 | 1.550 |
| three hexas/two quads | 2.000 | 2.400 | 3.600 | 3.640 | 1.553 |
| three hexas/three quads | 2.000 | 2.400 | 3.600 | 3.640 | 1.552 |
| one hexas/two trias | 2.000 | 2.400 | 3.600 | 3.640 | 1.554 |
| two hexas/two trias | 2.000 | 2.400 | 3.600 | 3.640 | 1.556 |

### *4.3 Square Plate with Circular Hole*

The third example problem is a square plate with a circular hole, as shown in Figure 11. The hole is small enough relative to the plate that additional elements, though not necessary, greatly improve convergence. In addition, because of the Poisson's effect, there will be some variation through the thickness. This example better illustrates how a global/local problem could be modeled, since the patch of shell elements around the hole is being replaced with solid elements, without modifying the mesh away from the hole.

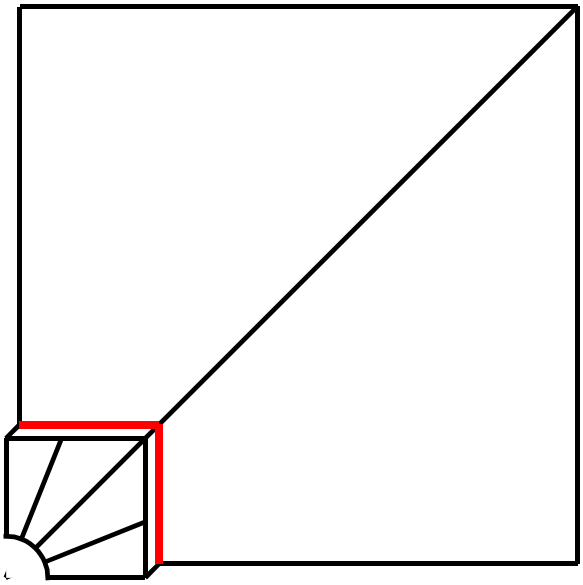

**Figure 11: Square Plate with Circular Hole.**

The square plate has a uniaxial tension load and symmetry constraints, so that the stress concentration factor at the hole may be calculated. Two transition interface elements were used, since the interface contains a right angle. The displacement contours and the von Mises stress contours for the four hexa/two quad mesh are shown on the deformed shapes in Figure 12.

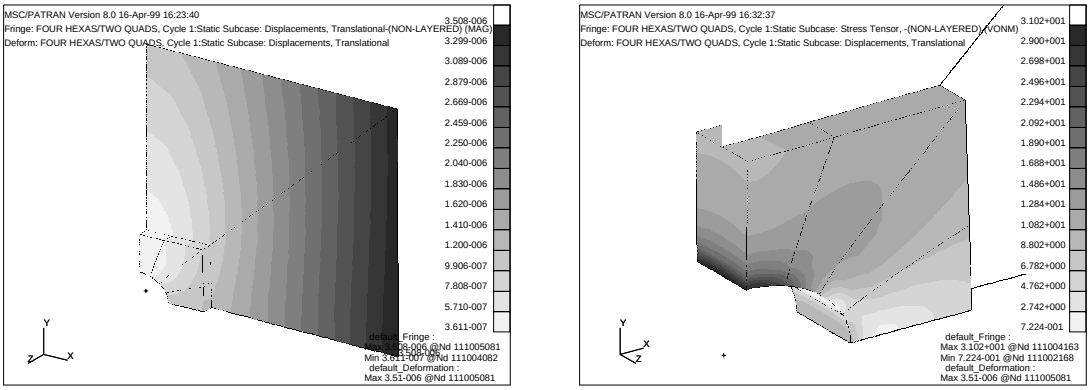


**Figure 12: Displacement and Stress Contours on Plate with Hole (p=8).**

The stress concentration factors at a sequence of p-levels are listed in Table 3 for four meshes with interface elements. The value calculated from [12] for a semi-infinite plate is 2.72, which is derived from curve fits to photoelastic data for a specified accuracy of "much less than 5%."

**Table 3: Stress Concentration Factor for Plate with Hole.**

| Mesh | p=3 | p=6 | p=8 |
|---|---|---|---|
| two hexas/two hexas | 2.955 | 2.760 | 2.787 |
| two hexas/three hexas | 2.748 | 2.786 | 2.794 |
| two hexas/four hexas | 2.761 | 2.784 | 2.792 |
| four hexas/four hexas | 2.735 | 2.783 | 2.792 |

The p=3 results are somewhat scattered, but the p=6 and p=8 results show that the two non-conforming meshes are much closer to the final conforming mesh than to the initial conforming mesh. This convergence of the stress concentration factors can be seen in Figure 13.

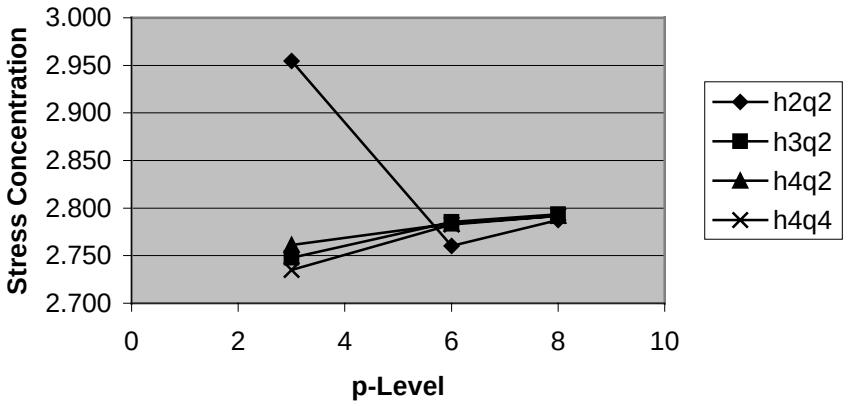


**Figure 13: Convergence of Stress Concentration Factors.**

This shows the advantage of the interface elements: adding additional solid elements in the primary area of interest using interface elements gives nearly the same answer as adding additional shell elements to make the mesh fully conforming.

# 5 Conclusions

Interface elements for dissimilar meshes are being implemented in MSC/NASTRAN. In the previous Part 1 [1] and Part 2 [2], curve interface elements were presented for shell and beam p-element edges along a geometric curve, and surface interface elements were presented for solid and shell p-element faces over a geometric surface, respectively. In the current Part 3, shell-to-solid transition interface elements are being presented for shell p-element faces and solid p-element edges. These elements are applicable to a wide range of problems, such as global/local analysis and component assembly. The transition interface elements use the hybrid variational formulation for the interface, developed by NASA Langley Research Center, and a Reissner-Mindlin formulation for the transition. This combination approach was summarized in this paper along with the implementation in MSC/NASTRAN.

Three sets of example problems were demonstrated, ranging from simple models having exact solutions to more complicated applications illustrating global/local analysis. The patch test and cantilever beam models showed that the transition interface elements provide the exact results for theoretical problems, whether or not the meshes are conforming. The plate with hole model showed that the interface elements can be used efficiently for global/local analysis, using more elements in the area of interest without having to transition to the model boundaries. The local area in that shell model was removed and replaced with a more refined solid mesh, and the results were nearly the same as having added shell elements to make the model fully conforming.

It is important to note that the interface elements provide a tool for connecting dissimilar meshes, but they do not increase the accuracy of the mesh. As with any interface formulation, the hybrid variational formulation, which imposes continuity conditions in a weak form, can not increase the accuracy of the adjacent boundaries. The Reissner-Mindlin formulation, which assumes plane sections remain plane, can not adequately describe a more complicated behavior. In addition, when a shell joins a solid, the behavior in the immediate vicinity is often dominated by fillets or other physical details, which are not modeled. These factors should be considered when deciding how close to the areas of primary interest to put the interface elements.

# 6 Acknowledgement

This work was performed in conjunction with NASA Cooperative Agreement NCC1-202, “Commercialization of NASA Interface Technology,” signed October 18, 1994, and NASA Cooperative Agreement NCC1-274, “Commercialization of NASA Interface Technology,” signed January 29, 1998.

# 7 References


1. J.E. Schiermeier, J.M. Housner, J.B. Ransom, M.A. Aminpour, and W.J. Stroud, "The Application of Interface Elements to Dissimilar Meshes in Global/Local Analysis," presented at the MSC 1996 World Users' Conference, Newport Beach, California, June 3-7, 1996.
2. J.E. Schiermeier, J.M. Housner, J.B. Ransom, M.A. Aminpour, and W.J. Stroud, "Interface Elements in Global/Local Analysis – Part 2: Surface Interface Elements," presented at the MSC 1997 Aerospace Users' Conference, Newport Beach, California, November 17-20, 1997.
3. M.A. Aminpour, J.B. Ransom, and S.L. McCleary, "Coupled Analysis of Independently Modeled Finite Element Subdomains," presented at the AIAA/ASME/ASCE/AHS/ASC 33rd Structures, Structural Dynamics, and Materials Conference, Dallas, Texas, April 13-15, 1992.
4. J.B. Ransom, S.L. McCleary, and M.A. Aminpour, "A New Interface Element for Connecting Independently Modeled Substructures," presented at the AIAA/ASME/ASCE/AHS/ASC 34th Structures, Structural Dynamics, and Materials Conference, La Jolla, California, April 19-21, 1993.
5. M.A. Aminpour, J.B. Ransom, and S.L. McCleary, "A Coupled Analysis Method for Structures with Independently Modelled Finite Element Subdomains," *International Journal for Numerical Methods in Engineering*, Vol. 38, pp. 3695-3718 (1995).
6. J.M. Housner, M.A. Aminpour, C.G. Dávila, J.E. Schiermeier, W.J. Stroud, J.B. Ransom, and R.E. Gillian, "An Interface Element for Global/Local and Substructuring Analysis," presented at the MSC 1995 World Users' Conference, Los Angeles, California, May 8-12, 1995.
7. M.A. Aminpour and T. Krishnamurthy, "A Two-Dimensional Interface Element for Multi-Domain Analysis of Independently Modeled Three-Dimensional Finite Element Meshes," presented at the AIAA/ASME/ASCE/AHS/ASC 38th Structures, Structural Dynamics and Materials Conference, Kissimmee, Florida, April 7-10 (1997).
8. C.G. Dávila, "Solid-to-Shell Transition Elements for the Computation of Interlaminar Stresses," *Computing Systems in Engineering*, Vol. 5, No. 2, pp. 193-202 (1994).
9. "MSC and NASA Agreement to Include NASA Technology in MSC/NASTRAN," *MSC/WORLD*, Vol. V, No. 1, pp. 23-24 (February 1995).
10. MSC/NASTRAN Quick Reference Guide Version 70.5, The MacNeal-Schwendler Corporation, Los Angeles, California (February 1998).
11. R.H. MacNeal and R.L. Harder, "A Proposed Standard Set of Problems to Test Finite Element Accuracy," *Finite Elements in Analysis and Design*, Vol. 1, pp. 3-20 (1985).
12. R.J. Roark and W.C. Young, *Formulas for Stress and Strain*, Fifth Edition, McGraw-Hill, Inc., New York (1975).